A TWO-DIMENSIONAL FINITE VOLUME MODEL IN NONORTHOGONAL COORDINATE SYSTEM

Chang-Wan Kim[1], Bong-Hee Lee[2], Yong-Sik Cho[3], and Tae Hoon Yoon[2]

[1]Water Resources and Environmental Research Division, Korea Institute of Construction Technology, Korea

[2]Department of Civil Engineering, Hanyang University, Korea

[3]Corresponding Author, Department of Civil Engineering, Hanyang University, Korea

Abstract: A two-dimensional flow model is newly developed. Two-dimensional shallow-water equations are discretized by the finite volume method. A nonorthogonal coordinate system is then employed. The developed model is applied to simulations of flows in a 180 degree curved bend flow. Numerical predictions are compared to available laboratory measurements. A good agreement is observed.

Key Words: shallow-water equations, finite volume method, nonorthogonal coordinate

1. INTRODUCTION

The finite volume method was firstly introduced in the field of computational fluid dynamics independently by McDonald(1971), and by MacCormack and Paullay(1972) to solve two-dimensional, time-dependent Euler equations. The method takes merits of both the finite difference and finite element methods. That is, in a sense, the finite volume method can be considered as a finite difference method applied to the differential conservative form of the conservation laws, written in arbitrary coordinate systems. Hence, this method can be applied by using an unstructured grid system as in the finite element method.

In general, the discretization of the governing equations in the control volume method can guarantee the conservation of mass, momentum and energy. Such conservation can be further sure to be the same as that in the original differential equations if the model is built based on the differential equations in a strong conservative form. This is probably the major advantage of the finite volume method. Furthermore, an additional numerical-source term is introduced if the shallow-water equations are discretized in a nonconserved form. For a continuous flow simulation, this additional numerical-source term has the same order of magnitude as the truncation error and it is usually negligible. However, for discontinuous flows, this term can become significantly large across the discontinuity and can cause serious errors (Hirsch, 1988).

The finite volume method is also known to

need less computational effort than the finite element method. Since the finite volume method is based on the integral form of the conservation equation, a conserved scheme can be easily constructed. As the space and time-step sizes approach zero, the scheme becomes consistent with the differential equations of conservation laws.

The main objective of this study is to present the development of a two-dimensional numerical model in a nonorthogonal curvilinear coordinate system to solve the two-dimensional shallow-water equations. In the following section, the shallow-water equations are introduced. Coordinate transformation is then described in section 3 and numerical scheme is presented in section 4. The boundary conditions employed in this study are also summarized in section 4. In section 5, the numerical model is tested by comparing the numerical solutions with existing laboratory measurements. Finally, concluding remarks are made in section 6.

2. GOVERNING EQUATIONS

Two-dimensional shallow-water equations can be written in the following conserved form (Yoon and Kim, 1996a)

$$\frac{\partial \zeta}{\partial t}+\frac{\partial (HU)}{\partial x}+\frac{\partial (HV)}{\partial y}=0 \tag{1}$$

$$\begin{aligned}&\frac{\partial (HU)}{\partial t}+\frac{\partial (UHU)}{\partial x}+\frac{\partial (VHU)}{\partial y}\\&=\frac{\partial}{\partial x}\left(H\nu^{t}\frac{\partial U}{\partial x}\right)+\frac{\partial}{\partial y}\left(H\nu^{t}\frac{\partial U}{\partial y}\right)-\\&gH\frac{\partial \zeta}{\partial x}+\frac{\tau_x^F}{\rho}-\frac{\tau_x^B}{\rho}\end{aligned} \tag{2}$$

$$\begin{aligned}&\frac{\partial (HV)}{\partial t}+\frac{\partial (UHV)}{\partial x}+\frac{\partial (VHV)}{\partial y}\\&=\frac{\partial}{\partial x}\left(H\nu^{t}\frac{\partial V}{\partial x}\right)+\frac{\partial}{\partial y}\left(H\nu^{t}\frac{\partial V}{\partial y}\right)-gH\frac{\partial \zeta}{\partial y}\\&+\frac{\tau_y^F}{\rho}-\frac{\tau_y^B}{\rho}\end{aligned} \tag{3}$$

where ζ is the free surface displacement. H is the total water depth defined as $H=h+\zeta$ with h being a still water depth. U and V are the depth-averaged horizontal velocity components. τ^F and τ^B are the shear stresses acting on the free surface and the channel bottom, respectively, ν^t represents the eddy viscosity, and ρ is the density of the fluid. The detailed description of the shear forces acting on the water surface and the channel bottom is given by Yoon and Kim(1996b).

If a linear distribution of shear stress has been assumed, the depth-averaged eddy viscosity used in the momentum equations is given by

$$\nu^{t}=\frac{\kappa}{6}U_{*}H \tag{4}$$

in which κ is the von *Ka'rma'n* constant, which is approximately equal to 0.4, and U_* is the shear velocity given by

$$U_{*}=\sqrt{gn^{2}\frac{V\sqrt{U^{2}+V^{2}}}{H^{1/3}}} \tag{5}$$

The momentum equations (2) and (3) can be generalized as

$$\begin{aligned}&\frac{\partial (H\phi)}{\partial t}+\frac{\partial (UH\phi)}{\partial x}+\frac{\partial (VH\Phi)}{\partial y}=\\&\frac{\partial}{\partial x}\left(H\varepsilon\frac{\partial \phi}{\partial x}\right)+\frac{\partial}{\partial y}\left(H\varepsilon\frac{\partial \phi}{\partial y}\right)+S_{\phi}\end{aligned} \tag{6}$$

in which ϕ is an arbitrarily dependent variable,

ε is the diffusion coefficient, which can stand either for the eddy viscosity of the momentum equations or for the eddy diffusion coefficient of the constituent transport equation, and S_ϕ denotes the source term of a dependent variable.

By considering a total flux consisted of the advection flux and diffusion flux, equation (6) can be rewritten as

$$\frac{\partial(H\phi)}{\partial t}+\frac{\partial J_x}{\partial x}+\frac{\partial J_y}{\partial y}=S_\phi \tag{7}$$

where J_x and J_y are defined as

$$J_x=HU\phi-H\varepsilon\frac{\partial\phi}{\partial x},\quad J_y=HV\phi-H\varepsilon\frac{\partial\phi}{\partial y} \tag{8}$$

3. COORDINATE TRANSFORMATION

In this section, a coordinate transformation is described. The generalized coordinate system used in this study is plotted in Figure 1. In the figure, a nonorthogonal coordinate system (ξ,η) is a function of $\xi(x,y)$ and $\eta(x,y)$. The contravariant vectors $\mathbf{e}^\xi$ and $\mathbf{e}^\eta$ are defined to be perpendicular to the surfaces where

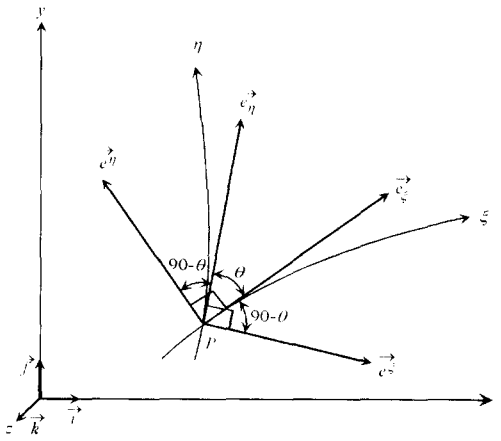

Fig. 1. A definition sketch of the nonorthogonal coordinate system

both ξ and η are constant. The covariant vectors $\mathbf{e}_\xi$ and $\mathbf{e}_\eta$ are defined to be tangent to the axes of ξ and η, respectively. The vectorized forms of the contravariant and covariant vectors are given in the following equations(Thompson *et al.*, 1985)

$$\mathbf{e}^\xi=\frac{1}{h_\eta}\left(\frac{\partial y}{\partial\eta}\mathbf{i}-\frac{\partial x}{\partial\eta}\mathbf{j}\right) \tag{9a}$$

$$\mathbf{e}^\eta=\frac{1}{h_\xi}\left(-\frac{\partial y}{\partial\xi}\mathbf{i}+\frac{\partial x}{\partial\xi}\mathbf{j}\right) \tag{9b}$$

$$\mathbf{e}_\xi=\frac{1}{h_\xi}\left(\frac{\partial x}{\partial\xi}\mathbf{i}+\frac{\partial y}{\partial\xi}\mathbf{j}\right) \tag{10a}$$

$$\mathbf{e}_\eta=\frac{1}{h_\eta}\left(\frac{\partial x}{\partial\eta}\mathbf{i}+\frac{\partial y}{\partial\eta}\mathbf{j}\right) \tag{10b}$$

where h_ξ and h_η are given by

$$h_\xi=\sqrt{\left(\frac{\partial x}{\partial\xi}\right)^2+\left(\frac{\partial y}{\partial\xi}\right)^2},\quad h_\eta=\sqrt{\left(\frac{\partial x}{\partial\eta}\right)^2+\left(\frac{\partial y}{\partial\eta}\right)^2} \tag{11}$$

Various relationships between the contravarient and covariant vectors, given in equations (9) and (10), could be derived as follows

$$\mathbf{e}_\eta\cdot\mathbf{e}^\xi=0,\quad \mathbf{e}^\eta\cdot\mathbf{e}_\xi=0,\quad \mathbf{e}_\eta\cdot\mathbf{e}_\xi=\cos\theta$$

$$\mathbf{e}^\eta\cdot\mathbf{e}^\xi=-\cos\theta,\quad \mathbf{e}^\xi\cdot\mathbf{e}_\xi=\sin\theta,\quad \mathbf{e}^\eta\cdot\mathbf{e}_\eta=\sin\theta \tag{12}$$

Let velocity vector in the Cartesian coordinates be $\mathbf{v}$ and the scalar product of $\mathbf{v}$ and $\mathbf{e}_\xi$, $\mathbf{e}^\xi$, $\mathbf{e}_\eta$, $\mathbf{e}^\eta$ be u_ξ, u^ξ, u_η, u^η, consecutively. Then, $\mathbf{v}$ can be expressed as

$$\mathbf{v} = \frac{h_\xi h_\eta}{J_a}\left(u_\xi \mathbf{e}^\xi + u_\eta \mathbf{e}^\eta\right) = \frac{h_\xi h_\eta}{J_a}\left(u^\xi \mathbf{e}_\xi + u^\eta \mathbf{e}_\eta\right) \tag{13}$$

where u^ξ and u^η can be expressed as functions of u_ξ and u_η given by

$$u^\xi = \frac{\alpha_\xi u_\xi - \beta_\xi u_\eta}{h_\eta}, \quad u^\eta = \frac{\alpha_\eta u_\eta - \beta_\eta u_\xi}{h_\xi} \tag{14}$$

and the following relationships have been used

$$J_a = \frac{\partial x}{\partial \xi}\frac{\partial y}{\partial \eta} - \frac{\partial y}{\partial \xi}\frac{\partial x}{\partial \eta}, \alpha_\xi = \frac{h_\xi h_\eta^2}{J_a}, \beta_\xi = \alpha_\xi \mathbf{e}_\xi \cdot \mathbf{e}_\eta,$$
$$\alpha_\eta = \frac{h_\eta h_\xi^2}{J_a}, \beta_\eta = \alpha_\eta \mathbf{e}_\xi \cdot \mathbf{e}_\eta \tag{15}$$

The gradients of function f in the directions of $\mathbf{e}_\xi$ and $\mathbf{e}_\eta$ are given as

$$\frac{\partial f}{\partial \xi} = h_\xi \nabla f \cdot \mathbf{e}_\xi, \quad \frac{\partial f}{\partial \eta} = h_\eta \nabla f \cdot \mathbf{e}_\eta \tag{16}$$

4. NUMERICAL SCHEME

The governing equations presented in the previous section are discretized by the finite volume method in this section. The notation system of Patankar(1980) has been adopted throughout this study. A typical control volume for node P is shown in Figure 2, where the uppercase letters denote the neighboring nodes and the lowercase letters represent the control volume faces.

The final discretized form of equation (6) is given by

$$a_P \phi_P = a_E \phi_E + a_W \phi_W + a_N \phi_N + a_S \phi_S + b + b_{NO} \tag{17}$$

The coefficients of equation (17) can be obtained from the following uniform format

$$a_E = a(P_e)D_e, \quad a_W = a(-P_w)D_w,$$
$$a_N = a(P_n)D_n, \quad a_S = a(-P_s)D_s \tag{18a}$$
$$a_P = a_E + a_W + a_N + a_S + F_e - F_w + F_n - F_s + H_P J_a \frac{\Delta\xi\Delta\eta}{\Delta t} \tag{18b}$$
$$b = S_\phi J_a \Delta\xi\Delta\eta + H_P^0 \phi_P^0 J_a \frac{\Delta\xi\Delta\eta}{\Delta t}, \quad b_{NO} = \hat{J}_e - \hat{J}_w + \hat{J}_n - \hat{J}_s \tag{18c}$$

in which $a(P) = \left[0,\ (1-0.1|P|)^5\right]$ is given by the

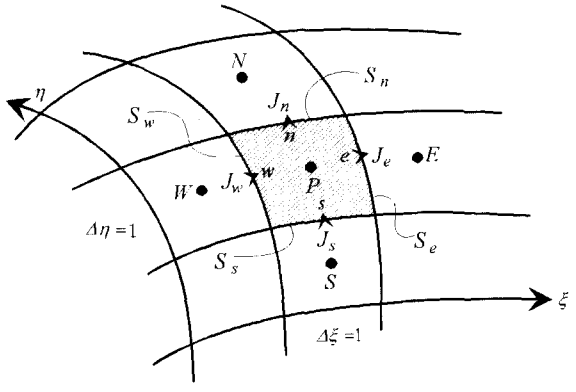

velocity and flux • depth

Fig. 2. A schematic sketch of a control volume in the nonorthogonal coordinate system

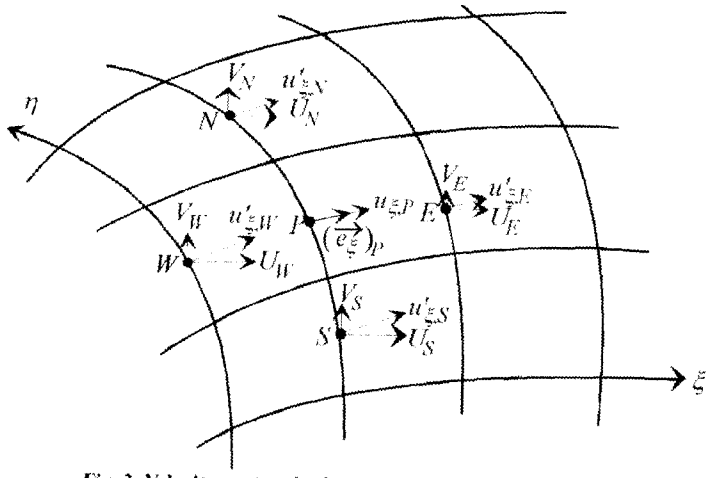

Fig. 3. Velocity vectors in the curvilinear coordinate system

power-law scheme, the superscript o denotes time step and the other terms are given as

$$F_e = H_e\left(\alpha_\xi u_\xi - \beta_\xi u_\eta\right)_e \Delta\eta_e,\quad F_\omega = H_\omega\left(\alpha_\xi u_\xi - \beta_\xi u_\eta\right)_\omega \Delta\eta_\omega$$
$$F_n = H_n\left(\alpha_\eta u_\eta - \beta_\eta u_\xi\right)_n \Delta\xi_n,\quad F_s = H_s\left(\alpha_\eta u_\eta - \beta_\eta u_\xi\right)_s \Delta\xi_s \tag{19a}$$

$$D_e = \frac{H_e\varepsilon_e\alpha_{\xi,e}}{\left(h_\xi\Delta\xi\right)_e},\quad D_\omega = \frac{H_\omega\varepsilon_\omega\alpha_{\xi,\omega}}{\left(h_\xi\Delta\xi\right)_\omega},$$
$$D_n = \frac{H_n\varepsilon_n\alpha_{\eta,n}}{\left(h_\eta\Delta\eta\right)_n},\quad D_s = \frac{H_s\varepsilon_s\alpha_{\eta,s}}{\left(h_\eta\Delta\eta\right)_s} \tag{19b}$$

$$\hat{J}_e = \beta_{\xi,e}\left(\frac{H\varepsilon}{h_\eta}\frac{\partial\phi}{\partial\eta}\right)_e,\quad \hat{J}_\omega = \beta_{\xi,\omega}\left(\frac{H\varepsilon}{h_\eta}\frac{\partial\phi}{\partial\eta}\right)_\omega$$
$$\hat{J}_n = \beta_{\eta,n}\left(\frac{H\varepsilon}{h_\xi}\frac{\partial\phi}{\partial\xi}\right)_n,\quad \hat{J}_s = \beta_{\eta,s}\left(\frac{H\varepsilon}{h_\xi}\frac{\partial\phi}{\partial\xi}\right)_s \tag{19c}$$

If ϕ is replaced by u_ξ or u_η in equation (19c), the equation becomes the momentum equation. As shown in Figure 3, $\mathbf{e}_\xi$s at E, W, N, and S may have different directions from that at P. The velocity components only parallel to $(\mathbf{e}_\xi)_P$ have to be considered. Thus, the momentum equation in the ξ-direction is written as

$$\begin{aligned} &a_P u_{\xi,P} \\ &= a_E u'_{\xi,E} + a_W u'_{\xi,W} + a_N u'_{\xi,N} + a_S u'_{\xi,S} + b + b_{NO} \\ &= a_E u_{\xi,E} + a_W u_{\xi,W} + a_N u_{\xi,N} + a_S u_{\xi,S} + b + b_{NO} \\ &+ a_E\left(u'_{\xi,E} - u_{\xi,E}\right) + a_W\left(u'_{\xi,W} - u_{\xi,W}\right) + a_N\left(u'_{\xi,N} - u_{\xi,N}\right) \\ &+ a_S\left(u'_{\xi,S} - u_{\xi,S}\right) \\ &= a_E u_{\xi,E} + a_W u_{\xi,W} + a_N u_{\xi,N} + a_S u_{\xi,S} + b + \\ &b_{NO} + b_C \end{aligned} \tag{20}$$

in which b_C is the additional term due to the curvature and $u'_{\xi,E} = \mathbf{v}_E \cdot (\mathbf{e}_\xi)_P$, $u'_{\xi,W} = \mathbf{v}_W \cdot (\mathbf{e}_\xi)_P$, $u'_{\xi,N} = \mathbf{v}_N \cdot (\mathbf{e}_\xi)_P$, and $u'_{\xi,S} = \mathbf{v}_S \cdot (\mathbf{e}_\xi)_P$.

The momentum equation in the η-direction can be also derived in the same manner.

The coupling between depth and velocity is done by the depth and velocity correction procedure analogous to the pressure and velocity correction procedure of the SIMPLER scheme(Patankar, 1980). The velocities calcu-

lated by the momentum equations may not exactly satisfy the continuty equation because the depth still remains as assumed.

To satisfy the continuity equation, a proper correction of depth and velocities is needed as follows

$$H = H^* + H' \tag{21a}$$

$$u_\xi = u_\xi^* + u'_\xi \tag{21b}$$

$$u_\eta = u_\eta^* + u'_\eta \tag{21c}$$

in which H' is a value of depth correction, u'_ξ and u'_η are values of velocity correction, and the superscript * denotes the value of a previous iteration step.

By applying equation (21) to the discretized continuity equation, the following first depth-correction equation can be obtained as

$$a_P H'_P = a_E H'_E + a_W H'_W + a_N H'_N + a_S H'_S + b + b_{NO} \tag{22}$$

where the coefficients are given as

$$a_E = H^*_e \alpha_{\xi,e} d_e \Delta\eta_e, \quad a_W = H^*_w \alpha_{\xi,w} d_w \Delta\eta_w,$$
$$a_N = H^*_n \alpha_{\eta,n} d_n \Delta\xi_n$$
$$a_S = H^*_s \alpha_{\eta,s} d_s \Delta\xi_s,$$
$$a_P = a_E + a_W + a_N + a_S + J_a \frac{\Delta\xi\Delta\eta}{\Delta t} \tag{23a}$$
$$b = -\left(H^*_P - H^0_P\right) J_a \frac{\Delta\xi\Delta\eta}{\Delta t} - H^*_e \alpha_{\xi,e} u^*_{\xi,e} \Delta\eta_e + H^*_w \alpha_{\xi,w} u^*_{\xi,w} \Delta\eta_w - H^*_n \alpha_{\eta,n} u^*_{\eta,n} \Delta\xi_n + H^*_s \alpha_{\eta,s} u^*_{\eta,s} \Delta\xi_s \tag{23b}$$
$$b_{NO} = H^*_e \beta_{\xi,e} u^*_{\eta,e} \Delta\eta_e - H^*_w \beta_{\xi,w} u^*_{\eta,w} \Delta\eta_w + H^*_n \beta_{\eta,n} u^*_{\xi,n} \Delta\xi_n - H^*_s \beta_{\eta,s} u^*_{\xi,s} \Delta\xi_s \tag{23c}$$

Because the depth-correction is related to the iterating velocities, the solution converges very slowly. To improve the convergence, another depth-correction equation, not related to the iterating velocities, is needed. Redefining $H = H^* + H''$ gives the other depth-correction equation expressed as

$$a_P H''_P = a_E H''_E + a_W H''_W + a_N H''_N + a_S H''_S + b + b_{NO} \tag{24}$$

where the coefficients except b and b_{NO} are the same as those given in equation (23), whereas b and b_{NO} are given as

$$b = -\left(H^*_P - H^0_P\right) J_a \frac{\Delta\xi\Delta\eta}{\Delta t} - H^*_e \alpha_{\xi,e} \hat{u}_{\xi,e} \Delta\eta_e + H^*_w \alpha_{\xi,w} \hat{u}_{\xi,w} \Delta\eta_w - H^*_n \alpha_{\eta,n} \hat{u}_{\eta,n} \Delta\xi_n + H^*_s \alpha_{\eta,s} \hat{u}_{\eta,s} \Delta\xi_s \tag{25a}$$
$$b_{NO} = H^*_e \beta_{\xi,e} \hat{u}_{\eta,e} \Delta\eta_e - H^*_w \beta_{\xi,w} \hat{u}_{\eta,w} \Delta\eta_w + H^*_n \beta_{\eta,n} \hat{u}_{\xi,n} \Delta\xi_n - H^*_s \beta_{\eta,s} \hat{u}_{\xi,s} \Delta\xi_s \tag{25b}$$

in which the pseudo-velocity $\hat{u}_{\xi,e}$ is defined in equation (26) and the other pseudo-velocities can be also defined in a similar manner.

$$\hat{u}_{\xi,e} = \frac{1}{a_e}\left(\sum a_{nb} u_{\xi,nb} + b + b_{NO} + b_C\right) - \left[\frac{g}{2a_e}\left(\frac{J_a \Delta\xi\Delta\eta}{h_\xi}\right)_e \left(H^*_E + H^*_P\right)\right] \left(H^*_E - H^*_P + Z_E - Z_P\right) \tag{26}$$

The flow regions are surrounded by a solid wall, inlet, and outlet. A slip boundary condition is applied to velocities on the wall, whereas Dirichlet or Neumann conditions have to be given properly according to the flow condition for the inlet and outlet. The boundary conditions

used in this study can be summarized as follows. That is, at the solid wall parallel with ξ-axis, the boundary conditions are given as

$$\frac{\partial u_\xi}{\partial \eta} = 0, \quad u_\eta = 0, \quad \frac{\partial H}{\partial \eta} = 0, \quad \frac{\partial \phi}{\partial \eta} = 0 \qquad (27)$$

At the solid wall parallel to η-axis, the boundary conditions are given as

$$u_\xi = 0, \quad \frac{\partial u_\eta}{\partial \xi} = 0, \quad \frac{\partial H}{\partial \xi} = 0, \quad \frac{\partial \phi}{\partial \xi} = 0 \qquad (28)$$

At the flow boundary where Dirichlet conditions are given, the boundary conditions are given as

$$u_\xi = u_{\xi,given}, \quad u_\eta = u_{\eta,given}, \quad H = H_{given}, \quad \phi = \phi_{given} \qquad (29)$$

At the flow boundary where Neumann conditions are given in the ξ-direction, the boundary conditions are given as

$$\frac{\partial u_\xi}{\partial \xi} = 0, \quad \frac{\partial u_\eta}{\partial \xi} = 0, \quad \frac{\partial H}{\partial \xi} = 0, \quad \frac{\partial \phi}{\partial \xi} = 0 \qquad (30)$$

At the flow boundary where Neumann conditions are given in the η-direction, the boundary conditions are given as

$$\frac{\partial u_\xi}{\partial \eta} = 0, \quad \frac{\partial u_\eta}{\partial \eta} = 0, \quad \frac{\partial H}{\partial \eta} = 0, \quad \frac{\partial \phi}{\partial \eta} = 0 \qquad (31)$$

In computations, the alternating direction implicit scheme is used to discretize those equations described previously.

5. NUMERICAL EXAMPLE

In this section, the performance of the developed model is examined by comparing numerical predictions to available laboratory measurements. Two examples are chosen: a flow in a 180° curved bend and a flow in a converging channel.

The numerical model is firstly applied to the simulation of flow in a bend. Obtained results are compared to laboratory measurements of the Shukry's 180° curved waterway (Shukry, 1950; Chow,1959).

In experiments, the width of a waterway is 0.3m, the lengths of straight reaches in both upstream and downstream are 1m, respectively, and the radius of the curvature in the bend is 0.15m. To reproduce the Shukry's experiment, a nonorthogonal curvilinear grid system was used. The width was divided in to 20 grids and the lengths of straight reaches were divided into 10 grids, while the length of the bend was divided into 18 grids with an angle of 10°. For flow in the bend, the boundary conditions at upstream are $u = 0.778$ m/sec and $v = 0$ m/s, whereas that at downstream is $H = 0.3$ m. In computation, the flow reaches an equilibrium state after about 200 iterations. The Manning roughness coefficient of 0.01 is used in the model.

In Figure 4, velocity vectors in the bend are plotted. Velocity vectors are parallel to x-axis at upstream, whereas they are curved along the bend and then parallel to x-axis again. Along the curved part, the magnitudes of velocity vectors along the inner bank are greater than those along the outer bank. This can be explained by the free vortex. That is, the magnitude of a velocity component is inversely proportional to the curvature of a channel.

Numerical solutions of the water surface levels along the inner and outer banks are displayed in Figure 5. Laboratory experimental measure-

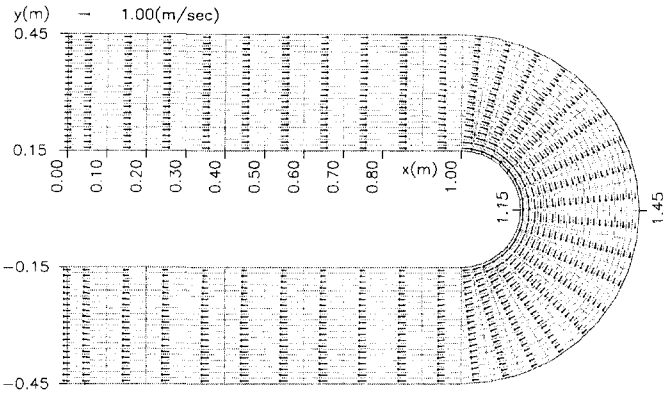

Fig. 4. Velocity components for the 180o bend flow

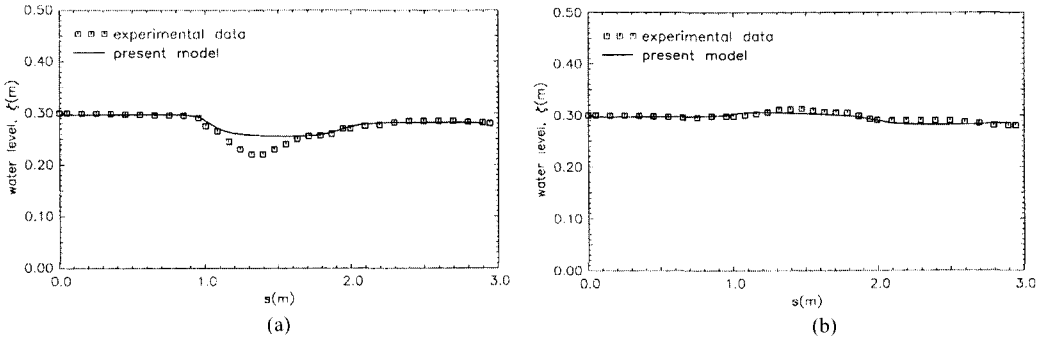

Fig. 5. Water surface elevation the 180o bend flow: (a) along the inner bank, (b) along the outer bank

ments are also plotted for a comparison. The agreement is reasonable along the outer bank as shown in Figure 5(a), while it is not good along the inner bank as shown in Figure 5(b). Specially, the disagreement is pronounced near the curved reach of the channel. This is probably because of the depth averaging property of the developed numerical model. However, the overall agreement is reasonable.

The model is secondly employed to investigate the behavior of the flow in a converging channel. Figure 6 shows the contour of depths in the converging channel used by Coles and Shintaku(1943). As shown in the figure, the channel is linearly converging from $x = 0.2980$ m to $x = 1.7780$ m. To model Coles and Shintaku's experiment, a nonorthogonal curvilinear grid system has also been used.

All 21 grids are used in the longitudinal direction, while 30 grids are used in cross-sectional direction(4 grids in the upstream, 20 grids in the converging part and 6 grids in the downstream). The Manning roughness coefficient is 0.007. The boundary conditions at upstream are $u = 2.25$ m/sec, $v = 0$ m/sec and $h = 0.319$ m. The Froude number is 1.27 and thus the flow regime at upstream is supercritical.

In Figure 7, contours of the surface elevation obtained from the developed model are plotted. The interval between two adjacent contours is 0.0025m. By comparing Figure 7 to Figure 6 a reasonable agreement is observed. Velocity

vectors in the converging channel are shown in Figure 8. The magnitude of the velocity is more or less constant. The water surface elevation is plotted in Figure 9. The elevation is increasing as the channel is converging as expected in a supercritical flow.

Finally, the water surface elevation along the centerline is shown in Figure 10. As the number of meshes increases the numerical prediction approaches closely laboratory measurements. Although the numerical model slightly underestimate elevations at $x = 1.4$m and 1.6m, the overall agreement is promising.

6. CONCLUDING REMARKS

In this study, a numerical model solving the two-dimensional shallow-water equations is developed. The model employs the finite volume method to discretize the governing equations in nonorthogonal curvilinear coordinate system.

Two examples whose laboratory measurements are available are employed to test the performance of the developed model. The computed predictions have been compared to available laboratory experimental data and the agreement between the computed and experimental results is reasonable. It was also shown that the model provides physically acceptable results although a coarse grid system is used.

ACKNOWLEDGEMENTS

This work presented in this paper was supported by funds of National Research Laboratory Program from Ministry of Science and Technology in Korea. Authors wish to appreciate the financial support.

REFERENCES

Chow, V.T. (1959). *Open-channel hydraulics*, McGraw-Hill Book Company.

Coles, D. and Shintaku, T. (1943). *Experimental relation between sudden wall angle changes standing waves in supercritical flow*, B.S. Thesis, Lehigh University, Pennsylvania, U.S.A.

Hirsch, C. (1988). Numerical computation of internal and external flows, Vol. 2, John Wiley & Sons.

MacCormack, R.W. and Paullay, A.J. (1972). "Computational efficiency acheived by time splitting of finite difference operators," *AIAA Paper 72-154*, American Institute of Aeronautics and Astronautics, San Diego, USA.

McDonald, P.W. (1971). "The computation of transonic flow through two-dimensional gas turbine cascades," *ASME Paper 71-GT-89*, American Society of Mechanical Engineers, New York, USA.

Patankar, S.V. (1980). *Numerical heat transfer and fluid flow. Hemisphere.*

Shukry, A. (1950). "Flow around bands in an open flume," *Transactions*, ASCE, Vol. 115, pp. 713-727.

Thompson, J.F., Warsi, Z.U.A. and Mastin, C.W. (1985). *Numerical grid generation: Foundations and applications*. Elsevier Science Publishing Co. Inc.

Yoon, T.H. and Kim, C.-W. (1996a). "Numerical analysis of two-dimensional horizontal flow by finite volume method: I. Development of a numerical model," *Journal of Korean Society of Civil Engineers*, Vol. 16, pp. 555-565.

Yoon, T.H. and Kim, C.-W. (1996b). "Numerical analysis of two-dimensional horizontal flow by finite volume method: II. Application of the numerical model," *Journal of Korean Society of Civil Engineers*, Vol. 16,

pp. 567-575.

Chang-Wan Kim, Water Resources and Environmental Research Division, Korea Institute of Construction Technology, Goyang, Kyeonggi 411-712, Korea

Bong-Hee Lee, Tae Hoon Yoon, Department of Civil Engineering, Hanyang University 17 Haengdang-dong, Seongdong-gu, Seoul 133-791, Korea

Yong-Sik Cho, Corresponding Author, Department of Civil Engineering, Hanyang University, 17 Haengdang-dong, Seongdong-gu, Seoul 133-791, Korea
(E-mail : ysc59@hanyang.ac.kr)

(Received March 7, 2001; accepted June 22, 2001)